Cubic interaction parameters for t_{2g} Wannier orbitals

T. Ribic, E. Assmann, A. Tóth, and K. Held

Institute of Solid State Physics, Vienna University of Technology, A-1040 Vienna, Austria
(Received 28 May 2014; revised manuscript received 10 September 2014; published 7 October 2014)

Many-body calculations for multi-orbital systems at present typically employ Slater or Kanamori interactions which implicitly assume a full rotational invariance of the orbitals, whereas the real crystal has a lower symmetry. In cubic symmetry, the low-energy t_{2g} orbitals have an on-site Kanamori interaction, albeit without the constraint $U = U' + 2J$ implied by spherical symmetry (U is the intra-orbital interaction, U' is the interorbital interaction, J is Hund's exchange). Using maximally localized Wannier functions we show that deviations from the standard, spherically symmetric interactions are indeed significant for $5d$ orbitals ($\sim$25% for BaOsO$_3$; $\sim$12% if screening is included) but are less important for $3d$ orbitals ($\sim$6% for SrVO$_3$; $\sim$1% if screened).

I. INTRODUCTION

Strongly correlated electron systems show a rich variety of unconventional phenomena such as high temperature superconductivity [1] and quantum criticality [2]—and their theoretical description and understanding constitutes a particular challenge. The origin of these correlations is the strong Coulomb interaction, as particularly found in materials with partially filled d or f bands, such as transition metals, their oxides, and rare-earth and lanthanide compounds.

The Coulomb interaction between two electrons, which scatter from orbitals α, β to α', β' in the course of the interaction, is simply given by

$$U_{\alpha'\beta'\beta\alpha} = \int d^3r \, d^3r' \, \psi_{\alpha'}^*(\mathbf{r}) \psi_{\beta'}^*(\mathbf{r}') V(|\mathbf{r}' - \mathbf{r}|) \psi_\beta(\mathbf{r}') \psi_\alpha(\mathbf{r}). \tag{1}$$

Here, $V(|\mathbf{r}' - \mathbf{r}|) = e^2/(4\pi\epsilon_0|\mathbf{r}' - \mathbf{r}|)$ is the Coulomb interaction with electron charge e and vacuum permittivity ϵ_0; $\psi_\alpha(\mathbf{r})$ is the electron wave function for orbital α; no screening by further electrons has been included in this bare interaction $U_{\alpha'\beta'\beta\alpha}$. We do not consider relativistic corrections such as the spin-orbit coupling here so that the one-electron eigenstates simply need to be multiplied with a spinor and the integrals $U_{\alpha'\beta'\beta\alpha}$ are independent of spin; however, the α' and α one-electron eigenstates (as well as β' and β) need to have the same spin.

For practical calculations, it is essential to reduce the number of interaction parameters. Often, e.g., in DFT + U (density-functional theory augmented by a Hubbard-U interaction in a static mean-field approximation) [3] and DFT + DMFT (dynamical mean-field theory) [4], one considers only the *local* interaction. That is, all orbitals α, β in Eq. (1) are on the same site; they might correspond to Wannier orbitals [5] localized around the same lattice site. This is justified not only because this on-site interaction is by far the largest interaction parameter, but also since nonlocal interactions between orbitals on different sites can be treated in simple (Hartree) mean-field theory in the limit of a large number of neighbors [6]. Certainly there are situations where such nonlocal interactions can be of importance, particularly in one and two dimensions, or also between transition-metal d and oxygen p orbitals [7].

A further reduction of parameters can be achieved by using the so-called Slater integrals [8]

$$F_l = \int dr \, dr' \, R(r)^2 R(r')^2 \frac{\min(r,r')^l}{\max(r,r')^{l+1}} r^2 r'^2. \tag{2}$$

Here, the underlying assumption is spherical symmetry, which allows for an analytical angular integration so that eventually only the integrals (2) over the radial part $R(r)$ of the wave functions remain; see the appendix. These Slater integrals, the simpler Kanamori [9] interaction, and or even just a single U parameter, are commonly used in DFT + U [10], DFT + DMFT [4,11–13], or full-multiplet configuration-interaction calculations [14–16]. However, a crystal lattice is not spherically symmetric. It has a lower, e.g., cubic, symmetry.

The aim of our paper is hence to analyze the nature and magnitude of the deviations from spherical interaction parameters. To this end, we study the specific and arguably most relevant case of transition-metal oxides with a cubic perovskite (ABO_3) structure. In Sec. II, we study analytically the structure of the Coulomb matrix elements for a BO_6 octahedron. For the low-energy t_{2g} orbitals, the cubic Coulomb interaction requires three parameters instead of the two parameters for spherical symmetry. We explicitly derive the most relevant integrals that deviate from the Slater integrals (2).

In Sec. III, we calculate the quantitative deviations from spherical symmetry by means of maximally localized Wannier orbitals. While the bare interaction in $3d^1$ SrVO$_3$ is still described reasonably well by spherically symmetric interaction parameters, the stronger p-d hybridization in $5d^4$ BaOsO$_3$ results in larger deviations ($\sim$25%). In a Wannier basis which includes both the transition-metal t_{2g} and oxygen p orbitals, working with spherically symmetric interactions is justified. Even for BaOsO$_3$, deviations between cubic and spherical symmetric interactions are only 3% in this case.

The effect of screening within the Thomas–Fermi approximation is considered in Sec. III C. For short screening lengths, deviations from spherical symmetry are even larger than in the unscreened case; for realistic screening lengths, deviations are reduced but still significant for BaOsO$_3$ in a three-orbital Wannier basis ($\sim$12%).

II. CUBIC INTERACTION PARAMETERS

We consider the typical situation for transition-metal oxides with an octahedron of oxygens surrounding each transition-metal atom, as shown in Fig. 1. While an isolated transition-metal atom would be spherically symmetric and the parametrization in terms of Slater integrals exact, the oxygen octahedron reduces the symmetry to cubic point group symmetry [17] around the transition-metal atom. Therefore, the fivefold degeneracy of the atomic d level is partially lifted, leaving a threefold degenerate t_{2g} and a twofold degenerate e_g level in the cubic environment. In the cases we consider, the octahedron vertices are occupied by negatively charged O^{2-} ions. In this case, the e_g states, which have a lot of weight along the B-O lines, are higher in energy than the t_{2g} states, whose weight resides predominantly in the space between the O ions; see Fig. 1(right).

The effective t_{2g} orbitals are a combination of predominantly transition-metal d orbitals admixed with oxygen p orbitals. For many transition-metal oxides, these t_{2g} orbitals constitute the low-energy degrees of freedom for excitations around the Fermi energy [18]. For an analytical description we consider an atomic transition-metal t_{2g} orbital, denoted d_α with $\alpha \in \{xy, yz, xz\}$ in the following. This d_α orbital mixes with a linear combination of oxygen p orbitals of the same symmetry; see, e.g., Ref. [15]. It is convenient to define this linear combination as o_α: e.g.,

$$o_{xy} = \left(p_x^{+y} + p_y^{+x} - p_x^{-y} - p_y^{-x}\right)/2, \qquad (3)$$

where p_x^{+y} is the p_x orbital centered around the oxygen atom in the the positive y direction; see Fig. 1. The orbitals o_{xz} and o_{yz} follow from Eq. (3) by cubic symmetry, i.e., $x \leftrightarrow z$ and $y \leftrightarrow z$, respectively.

Symmetry ensures that the orbital o_α is orthogonal to $d_{\alpha'}$, except when $\alpha = \alpha'$. Thus to orthogonalize the set of orbitals $\{o_\alpha, d_{\alpha'}\}$, one has only to orthonormalize o_α with respect to its associated d_α. The orthonormalized orbitals are

$$o'_{\alpha=ij} = \frac{o_{ij} - d_{ij}\langle d_{ij}|o_{ij}\rangle}{\sqrt{1 - \langle d_{ij}|o_{ij}\rangle}}. \qquad (4)$$
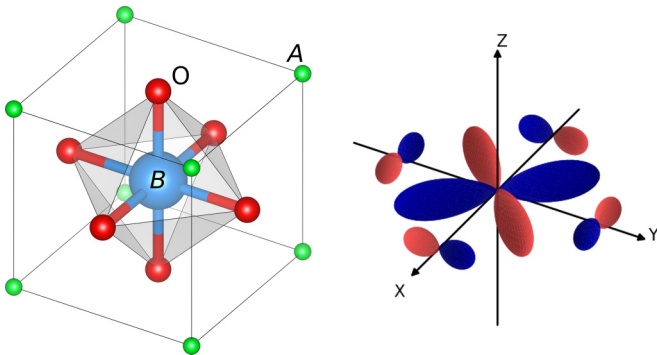
FIG. 1. (Color online) (left) In the perovskite ($A B$O$_3$) structure, the oxygen octahedron around the central transition-metal ion breaks spherical symmetry down to cubic. The B ion (large sphere) occupies the center of a cube with A at the corners and O at the face centers. (right) Schematic representation of the low-energy d'_{xy} orbital of Eq. (5) [light and dark shading indicates opposite signs of the wave function].

The mixing of transition-metal d orbitals and oxygen p orbitals stems from hybridization; by symmetry, there is a hybridization only between d_α and o'_α with the same α. Hence we obtain the tight-binding Hamiltonian

$$\begin{pmatrix} E_d & t \\ t & E_p \end{pmatrix},$$

where E_d and E_p are the d and p (more precisely the orthogonalized o') energy levels; $E_d - E_p$ is the charge transfer energy. The predominantly d eigenfunctions of this tight-binding Hamiltonian, d'_{ij}, are the effective low-energy t_{2g} orbitals

$$d'_{ij} = a d_{ij} + b o'_{ij}, \qquad (5)$$

with $\eta = (E_d - E_p)/(2t)$, $a = [2(\eta^2 - \eta\sqrt{\eta^2+1} + 1)]^{-1/2}$, and $b = [2(\eta^2 + \eta\sqrt{\eta^2+1} + 1)]^{-1/2}$.

After defining the low-energy t_{2g} orbitals, we need to calculate the Coulomb interaction between these one-particle eigenstates, i.e.,

$$U_{\alpha'\beta'\beta\alpha} = \langle d'_{\alpha'=ij}|\langle d'_{\beta'=kl}|V|d'_{\beta=mn}\rangle|d'_{\alpha=op}\rangle. \qquad (6)$$

This is the relevant site-local Coulomb interaction for the low-energy degrees of freedom. Note that, in this context, $U_{\alpha'\beta'\beta\alpha}$ is defined as the matrix element between direct products of single-particle states denoted as $|d'_{\beta=mn}\rangle|d'_{\alpha=op}\rangle$, not between antisymmetrized Fock states.

Since often $b \ll 1$ in transition-metal oxides, we consider in the following only the leading terms in the limit of large distance between transition-metal and oxygen sites. In this limit, the direct overlap $\langle d_{ij}|o_{ij}\rangle$, b (which is the overlap with respect to the one-particle Hamiltonian, $b \sim t$), and Coulomb integrals between orbitals on different sites are small. In the following we hence restrict ourselves to all terms up to second order in (any) of the above off-site overlaps and obtain the following three contributions:

Directly from the $a d_{ij}$ terms in Eq. (5) and from the orthogonalization of the o'_{ij} we get a contribution

$$\left(a^4 - 4a^3 b \frac{\langle d_{uv}|o_{uv}\rangle}{N}\right)\langle d_{ij}|\langle d_{kl}|V|d_{mn}\rangle|d_{op}\rangle. \qquad (7)$$

This term is centered around the transition-metal ion and can be expressed in terms of the Slater integrals F_l for the d_{ij} orbitals. Hence, this term can still be parametrized with Kanamori interaction parameters.

From two $b o'_{ij}$s in Eq. (5) we get a contribution

$$\left(2a^2 b^2 \frac{1}{N^2}\right)\langle d_{ij}|\langle o_{kl}|V|o_{mn}\rangle|d_{op}\rangle. \qquad (8)$$

Note that o_{kl} and o_{mn} have a contribution from the same oxygen site, so that the r and r' integrals both include on-site overlaps. Since for large oxygen–transition-metal distances the intersite overlap decays exponentially while the Coulomb interaction decays like $1/r$, we keep the term Eq. (8).

Finally, there is a contribution involving only one $b o'_{ij}$ in Eq. (5) and a Coulomb integral overlap between transition-metal and oxygen sites:

$$\left(2a^3 b \frac{1}{N}\right)\langle d_{ij}|\langle d_{kl}|V|o_{mn}\rangle|d_{op}\rangle. \qquad (9)$$

All other terms are of higher order in b or the off-center overlap integrals.

Equations (8) and (9) involve Coulomb integrals with two distinct sites, oxygen and transition metal. Hence, they cannot be expressed in terms of Slater integrals any longer. One can also envisage this from the orbital in Fig. 1(right). While the spherical rotations around the x or y axis of the central d_{xy} part of the d'_{xy} orbital in Fig. 1(right) map the d_{xy} orbital onto a linear combination of the three d_α orbitals, this is not possible any longer with the oxygen admixture o'_{xy} in d'_{xy} except for 90 degree rotations. Noncubic rotations will put the rotated orbitals into positions where there is actually no oxygen site.

Employing the cubic symmetry, we can further reduce the number of integrals needed in Eqs. (7)–(9); or (1); cf. Ref. [19]. Any integral involving an orbital index $\alpha = ij$ once or thrice is odd in one cubic direction and hence vanishes. This leaves us with integrals where all orbitals are the same, i.e., the intra-orbital Hubbard interaction $U = U_{\alpha\alpha\alpha\alpha}$ and integrals where we have two distinct orbitals $\alpha \neq \beta$ twice. For the latter we have three possibilities: the interorbital interaction $U' = U_{\alpha\beta\beta\alpha}$, the Hund's exchange $J = U_{\alpha\beta\alpha\beta}$, the pair hopping term and $U_{\alpha\alpha\beta\beta}$ which, for real-valued wave functions, has the same amplitude as J. These symmetry considerations actually hold in general, but without spherical symmetry $U \neq U' + 2J$ because of the terms (8) and (9). For spherical symmetry, the connection to the Slater integrals is as follows (cf. Ref. [19]): $U = F_0 + \frac{4}{49}(F_2 + F_4)$, $U' = F_0 - \frac{2}{49}F_2 - \frac{4}{441}F_4$, $J = \frac{3}{49}F_2 + \frac{20}{441}F_4$, so that $U = U' + 2J$ holds [20]. If we have instead only cubic symmetry, we can still parametrize the interaction in terms of U, U', and J, but now with $U \neq U' + 2J$ and no expression in terms of Slater integrals.

In second quantization, this Kanamori Hamiltonian [9], which is obtained from Eq. (1) by including all valid spin combinations in Eq. (1), reads

$$
\begin{aligned}
H_U &= \frac{1}{2} \sum_{\substack{\alpha,\beta \\ \alpha',\beta'}} U_{\alpha'\beta'\beta\alpha} \sum_{\sigma,\sigma'} c^\dagger_{\alpha'\sigma} c^\dagger_{\beta'\sigma'} c_{\beta\sigma'} c_{\alpha\sigma} \\
&= U \sum_\alpha n_{\alpha,\uparrow} n_{\alpha,\downarrow} + \sum_{\substack{\alpha>\beta \\ \sigma,\sigma'}} [(U' - \delta_{\sigma\sigma'}J)n_{\alpha,\sigma} n_{\beta,\sigma'}] \\
&\quad - \sum_{\alpha \neq \beta} J(c^\dagger_{\alpha,\downarrow} c^\dagger_{\beta,\uparrow} c_{\beta,\downarrow} c_{\alpha,\uparrow} + c^\dagger_{\beta,\uparrow} c^\dagger_{\beta,\downarrow} c_{\alpha,\uparrow} c_{\alpha,\downarrow} + \text{H.c.}).
\end{aligned}
\tag{10}
$$

Here, $c^\dagger_{\alpha,\sigma}$ ($c_{\alpha,\sigma}$) creates (annihilates) an electron with spin σ in orbital α; $n_{\alpha,\sigma} = c^\dagger_{\alpha,\sigma} c_{\alpha,\sigma}$.

In contrast, for the e_g orbitals, which are proportional to $3z^2 - r^2$ and $\sqrt{3}(x^2 - y^2)$, the relation $U = U' + 2J$ still holds for cubic symmetry: Again because of cubic symmetry ($x \leftrightarrow y$) any term involving one or three $x^2 - y^2$ orbitals vanishes; only the terms $U = U_{\alpha\alpha\alpha\alpha}$, $U' = U_{\alpha\beta\beta\alpha}$, $J = U_{\alpha\beta\alpha\beta} = U_{\alpha\alpha\beta\beta}$ remain. However, now, instead of interchanging the orbitals, cubic symmetry operations such as ($x \to x$, $y \to z$, $z \to -y$), lead to mixed orbitals: $3z^2 - r^2 \to -1/2(3z^2 - r^2) - \sqrt{3}/2\sqrt{3}(x^2 - y^2)$. Hence, the intra-orbital Hubbard interaction U for the e_g orbitals is not a cubic invariant, and

U has to depend on the other parameters U' and J through $U = U' + 2J$.

III. QUANTITATIVE DEVIATIONS FOR SrVO$_3$ AND BaOsO$_3$

A. Construction of Wannier functions

We now aim to validate our analytical results and quantify the deviation from the spherical-symmetry relationship (1) in real materials. To this end, we perform DFT calculations [21] by using a generalized-gradient approximation to the exchange-correlation functional [22] for two cubic perovskite materials and construct low-energy effective models using maximally localized Wannier functions (MLWFs) [23,24].

In terms of the formalism of Sec. II, the role of the Wannier functions is to provide the radial dependence of the orbitals which was irrelevant for our arguments from symmetry, but which must be provided to compute numerical values for the interaction parameters. The main difference is that we considered a local octahedron before, while Wannier functions $|w_{\alpha\mathbf{R}}\rangle$ properly belong to a periodic crystal: they have finite hopping amplitudes $t_{\alpha\mathbf{R}\alpha'\mathbf{R}'}$ also for $\mathbf{R} \neq \mathbf{R}'$ (or equivalently, they show a $\mathbf{k}$ dispersion) and form an orthonormal set $\langle w_{\alpha\mathbf{R}} | w_{\alpha'\mathbf{R}'} \rangle = \delta_{\alpha\alpha'} \delta_{\mathbf{R}\mathbf{R}'}$ with respect to sites $\mathbf{R}$ and orbitals α.

Our first example is SrVO$_3$, which is often used as a "test bed" strongly correlated material. (For DFT + DMFT calculations; see, e.g., Ref. [25]. Detailed discussions of Wannier projections in this and related materials are given in Refs. [24,26,27].) The cubic perovskite SrVO$_3$ is a paramagnetic, correlated metal with electronic configuration $3d^1$, i.e., one of the t_{2g}-derived states will be filled.

Second, we consider the recently synthesized compound BaOsO$_3$ [28]. With a low-spin $5d^4$ configuration, this is another paramagnetic metal. Since the $5d$ states are more extended than the $3d$ states of V, we expect to find greater p-d hybridization and, in turn, greater deviation from $U = U' + 2J$ in this case.

For each material, we construct two sets of Wannier functions:

(1) three "d-only" Wannier functions corresponding to the d'_{ij} of Eq. (5), and

(2) twelve "$d + p$" Wannier functions corresponding to the atomic d_{ij} and p_i states.

It is instructive to compare these two approaches: The first set of Wannier functions translates the three t_{2g}-derived bands to three orbitals $|w'_{\alpha\mathbf{0}}\rangle$ centered on the B ion. Direct and O-mediated hopping processes are subsumed in an effective B-B hopping $t_{d'd'}$. To account for this, $|w'\rangle$ must have substantial weight not only at B but also at O atoms. (In a band picture, the reason is the significant O-p contribution to the t_{2g}-derived bands.) Which combinations of O-p and B-d orbitals mix is determined by symmetry, as discussed in Sec. II; cf. Fig. 2. Going beyond an effective single-particle description, the Coulomb interaction is expected to be well represented by a site local "multiband Hubbard" term $U_{\alpha'\beta'\beta\alpha}$ which can be parametrized by three independent quantities U, U', and J, as we saw in the previous section.
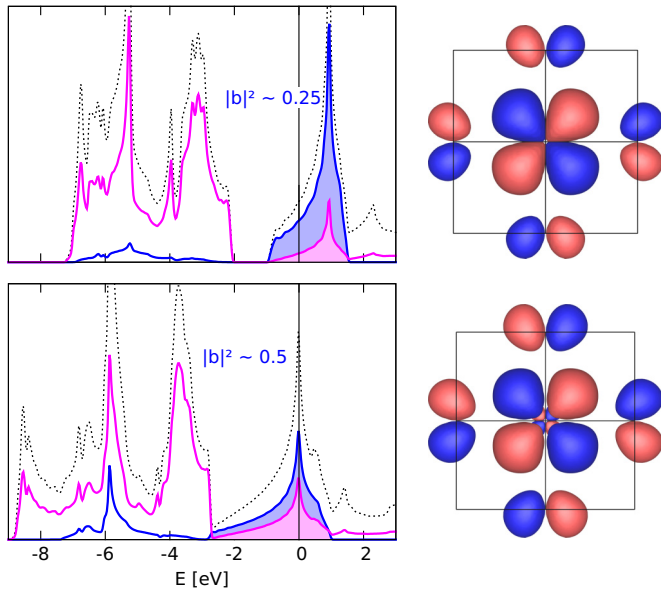
FIG. 2. (Color online) Densities of states and Wannier functions for the d-only Wannier orbitals for $SrVO_3$ (top) and $BaOsO_3$ (bottom). On the left, we show the total DOS (dotted line) and the projections on transition-metal t_{2g} (dark) and O (light) states. The shaded area marks the region of integration used to estimate the O-p weight [corresponding to $|b|^2$ in Eq. (5)], see text. On the right, the light (dark) lobes are isosurfaces for the positive (negative) parts of the real-valued Wannier functions. The strong p-t_{2g} hybridization and the antibonding character are plainly visible.

The second set of Wannier functions spans nine additional bands: three p-derived bands per O. With the p states explicitly included, the d-like MLWFs are free to become more localized; the weight at the O sites will be carried by the p-like orbitals (cf. Fig. 3). The downside is that the resulting model becomes significantly more complex, since a correct treatment of such a $d + p$ model must take into account not only the intra-atomic interactions on the B (U_{dd}) and on the O (U_{pp}) sites, but also the interatomic (U_{pd}) interactions [7,29]. This added complexity will increase the computational cost to solve the model in any numerical method, but it will also make the physical interpretation of the results more involved.

Before we turn to the results, note that the heavy ($Z = 76$) element Os leads to an appreciable spin-orbit splitting in $BaOsO_3$. Because it would invalidate the symmetry analysis of Sec. II, we neglect this effect in the construction of the Wannier functions. While our analysis could be extended to include spin-orbit coupling, a spin-orbit interaction term can also be added afterwards to the tight-binding model in any case [30].

B. Results

Figure 2 shows the densities of states (DOS) of $SrVO_3$ and $BaOsO_3$, and the Wannier orbitals corresponding to the three-band case. The DOS around the Fermi level is derived from the π-antibonding combinations of O-p and B-t_{2g} states; correspondingly, the three-band orbitals are composed of a d-like contribution at the B site and p-like contributions at the O sites sharing a plane with the d-like part, akin to the o'_α
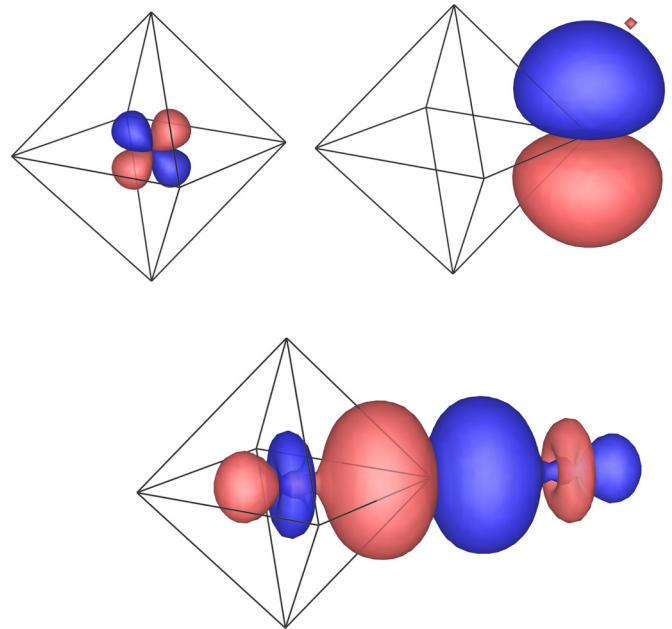
FIG. 3. (Color online) Twelve-orbital Wannier functions for $SrVO_3$ [plotted as in Fig. 2(right)]. (top left) By symmetry, the twelve orbitals are grouped into three equivalent d-like orbitals; and two types of p-like orbitals, (bottom) three "p_σ" whose symmetry axes point toward their B neighbors, and (top right) six "p_π" pointing away from the B sites. With the O-p states explicitly included, no p-t_{2g} hybridization is seen in these orbitals. Correspondingly, the d and p_π orbitals are close to their atomic counterparts. Conversely, the p_σ orbitals, which mediate the σ bonding between O-p and B-e_g states, are elongated along their symmetry axis and have large contributions at their B neighbors [26,27].

orbitals in Sec. II. These Wannier orbitals are also referred to as d only, where the quotation marks hint that these orbitals are actually not pure d orbitals. The Wannier functions are equivalent to each other under cubic symmetry.

As expected, the p-d hybridization is stronger in $BaOsO_3$ than in $SrVO_3$. This is seen both in the DOS (more O weight around the Fermi energy $E_F = 0$) and in the orbitals (bigger lobes at the O sites). We can quantify this observation by integrating over the shaded areas in the DOS; this yields an O admixture of $|b_{SrVO_3}|^2 \sim 0.25$ and $|b_{BaOsO_3}|^2 \sim 0.5$, respectively. In this sense, the "d bands" of $BaOsO_3$ consist in fact of almost equal parts O and Os contributions. These values agree qualitatively with Eq. (5), which yields $|b_{SrVO_3}|^2 \sim 0.20$ and $|b_{BaOsO_3}|^2 \sim 0.33$ using the parameters from Table VI [31]. Quantitative differences have to be expected because (i) Eq. (5) holds for an isolated octahedron instead of the periodic crystal, (ii) there are further hopping integrals that would have to be considered, and (iii) the partial DOS of Fig. 2 are only projections within the muffin-tin spheres [21].

For these d-only Wannier orbitals, we calculated the Coulomb interaction by spatial integration of Eq. (1) [32]. Table I summarizes the results obtained for the bare interaction. For the $3d^1$ perovskite $SrVO_3$, deviations from the spherical symmetric relation $U - U' = 2J$ are 6%. That is, calculations employing this relation can still be expected to yield quite reliable results. For the $5d^4$ perovskite $BaOsO_3$, on the other

TABLE I. Coulomb interactions (unscreened) for d-only Wannier functions of SrVO$_3$ and BaOsO$_3$; $(U - U')/2 = J$ holds for spherical but not for cubic symmetry, for BaOsO$_3$ deviations are indeed substantial.

Interaction	SrVO$_3$	BaOsO$_3$
U	16.30 eV	10.54 eV
U'	15.14 eV	9.67 eV
J	0.55 eV	0.33 eV
$(U - U')/2$	0.58 eV	0.44 eV

hand, deviations are 25%. The reason for this is the larger admixture of oxygen p contributions, which according to Sec. II yield larger off-center Coulomb integral overlaps and hence a larger deviation from spherical symmetry.

Recently, transition-metal oxides with heavy $4d$ or $5d$ elements have attracted more and more attention. Indeed, in such systems electronic correlations are stronger than expected—due to Hund's rule coupling [19,33,34]. All the more important is a correct Hamiltonian and multiplet structure with Hund's exchange. In this respect, our finding highlights the substantial difference between $(U - U')/2$ and J. A Kanamori Hamiltonian with three independent Coulomb interactions needs to be considered for obtaining the correct multiplet structure.

Next, we turn to the twelve-orbital $d + p$ Wannier functions. This is an alternative description of the low-energy physics, where the oxygen p orbitals are explicitly taken into account. The corresponding Wannier functions for SrVO$_3$ are shown in Fig. 3. The d-like orbitals are again equivalent up to symmetry, but two inequivalent types of p-like orbitals appear. Symmetry also greatly restricts the possible hopping processes between these states. The hopping amplitudes within the octahedron as well as selected longer-ranged ones for all four Wannier projections are reported in Appendix B.

We list the Coulomb interaction parameters between the twelve-band orbitals for SrVO$_3$ and BaOsO$_3$ in Tables II and III, respectively. For the d-like orbitals, $U = U' + 2J$ is fulfilled with a reasonable accuracy of 3% even in BaOsO$_3$. Having the additional degree of freedom regarding oxygen-p Wannier orbitals, the t_{2g} orbitals are now localized around the transition-metal ion and have the spherically symmetric form; cf. Fig. 3. In this case, two parameters are sufficient for the d-d Kanamori interaction.

TABLE II. Left: Same as Table I but for $d + p$ SrVO$_3$ Wannier functions. Right: the different d-p density-density Coulomb interactions for these Wannier functions; see main text for the notation.

Interaction	SrVO$_3$	Interaction	SrVO$_3$
U	19.99 eV	$U_{p_\pi d}$	7.24 eV
U'	18.52 eV	$U'_{p_\pi d}$	7.18 eV
J	0.74 eV	$U_{p_\sigma d}$	8.52 eV
		$U^\perp_{p_\sigma d}$	6.87 eV
$(U - U')/2$	0.74 eV	$U^\perp_{p_\pi d}$	8.06 eV

TABLE III. Same as Table II but for $d + p$ BaOsO$_3$ Wannier functions.

Interaction	BaOsO$_3$	Interaction	BaOsO$_3$
U	14.90 eV	$U_{p_\pi d}$	6.94 eV
U'	13.65 eV	$U'_{p_\pi d}$	6.80 eV
J	0.64 eV	$U_{p_\sigma d}$	7.85 eV
		$U^\perp_{p_\sigma d}$	7.23 eV
$(U - U')/2$	0.62 eV	$U^\perp_{p_\pi d}$	6.38 eV

As a side note, observe that in the twelve-band case $U - U' < 2J$, while in the three-band case $U - U' > 2J$. This is because U' and J are more strongly reduced than U by the shift of t_{2g} weight to the oxygens which occurs in the three-band case, as U' and J are *inter*orbital interactions that include more nonoverlapping oxygens in the interaction integral.

Let us emphasize that the d-p interaction also plays an important role [29]. The d-p interactions of density-density type are listed in Tables II and III (right). There are two types of p orbitals, denoted p_π and p_σ (see Fig. 3). Interactions with p orbitals centered on an oxygen atom outside the plane of the d orbital lobes are denoted by $\perp$. The d-p_σ interactions $U_{p_\sigma d}$ and $U^\perp_{p_\sigma d}$ with the p_σ orbitals oriented toward the transition-metal site is considerably stronger than that with the more regular p_π orbitals. There is only one $U^\perp_{p_\pi d}$, while two parameters arise from density-density interaction between d and p_π orbitals with the p_π orbitals being centered around oxygen sites within the plane defined by the d orbitals. We denote these as $U_{p_\pi d}$ if the p_π orbital lies within the same plane and $U'_{p_\pi d}$ if it is oriented perpendicular to it. The considerable differences in the d-p Coulomb interaction can be understood from the very different p_π and p_σ orbitals in Fig. 3. These differences are of relevance for $d + p$ DFT + DMFT calculations that include U_{pd} [29].

C. Effect of screening

The values reported above were calculated for a bare, unscreened Coulomb interaction. In this section we include screening, within Thomas–Fermi theory. That is, we replace the bare interaction in Eq. (1) by

$$V(|\mathbf{r}' - \mathbf{r}|) = \frac{e^2}{4\pi\epsilon_0} \frac{1}{|\mathbf{r}' - \mathbf{r}|} e^{-|\mathbf{r}' - \mathbf{r}|/\lambda_{\mathrm{TF}}}, \quad (11)$$

where λ_{TF} is the Thomas–Fermi screening length. Let us emphasize that, for a cubic crystal, the screened interaction $V(\mathbf{r}, \mathbf{r}')$ itself will be of cubic symmetry and hence deviate from spherical symmetry. This effect is not taken into account in the following; it will on its own generate further deviations of the Kanamori interaction parameters from the spherical relation $U = U' + 2J$.

In the following, we adjust the parameter λ_{TF} to yield a screened Coulomb interaction $U' \sim 3.5$ eV for $3d$ SrVO$_3$, as calculated using the constrained local density approximation [25]. This corresponds to a screening length $\lambda_{\mathrm{TF}} = 0.43$ Å (the lattice parameters are $a_{\mathrm{SrVO_3}} = 3.8425$ Å [35] and $a_{\mathrm{BaOsO_3}} = 4.025$ Å [28]). We employ the same screening length

TABLE IV. Same as Table I but for screened interaction with screening length $\lambda_{\mathrm{TF}} = 0.43$ Å.

Interaction	SrVO$_3$	BaOsO$_3$
U	4.40 eV	2.44 eV
U'	3.47 eV	1.80 eV
J	0.46 eV	0.28 eV
$(U - U')/2$	0.47 eV	0.32 eV

also for BaOsO$_3$ because this yields an interaction parameter $U' \sim 1.8$ eV, which is in the expected range for the 5d BaOsO$_3$.

Table IV shows the results obtained for the d-only models. In the case of 3d orbitals, as exemplified by SrVO$_3$, deviations from spherically symmetric interaction parameters are already small without screening and become negligible if screening is included. By contrast, for 5d BaOsO$_3$, $U - U' = 2J$ is significantly violated even when screened. Let us note that the degree of deviation is quite robust over a large range of screening lengths. For example with $\lambda_{\mathrm{TF}} = 0.61$ Å we obtain a similar deviation of 14% ($U = 2.55$ eV, $U' = 1.90$ eV, and $J = 0.28$ eV).

Interestingly, for weak screening (large λ) J can even be enhanced whereas U and U' are always reduced. The reason for this is that the exchange integral J includes positive *and* negative contributions; and for large λ_{TF}, the negative contributions are more strongly reduced than the positive ones. For example, at $\lambda_{\mathrm{TF}} = 21.13$ Å we obtain $J = 0.5465$ eV for SrVO$_3$, which is larger than the unscreened $J = 0.5464$ eV. As the increase is very small, the results are given to a higher precision than elsewhere in the paper. With $U = 15.67$ eV and $U' = 12.50$ eV, deviations are 6.2% for this screening strength.

In the limit of infinite screening, i.e., $\lambda_{\mathrm{TF}} \to 0$, one can show that $U' = J$. That is, one can describe this limit by one Kanamori interaction parameter $U = 3U' = 3J$ for spherical symmetry, and two (U and $U' = J$) for cubic symmetry. Numerically, we get, however, also for cubic d-only Wannier functions, $U/J \sim 3$ for both SrVO$_3$ and BaOsO$_3$. The limits of strong and weak screening show that the idea that screening strongly reduces U' and hardly reduces J is not true in general. For strong screening, J is reduced as much as U', since they are equal, while for weak screening J is even enhanced.

IV. CONCLUSION

We analyzed the physical origin and the magnitude of the difference between a spherically symmetric and a cubic interaction for t_{2g} orbitals. Deviations are quite large for 5d orbitals of heavy transition metals. Since for these systems Hund's exchange is paramount for electronic correlations [12,19,34,36], we conclude that a Kanamori interaction with three instead of two independent parameters is necessary. Unfortunately, this requires the calculation of one additional interaction parameter and hence a more thorough analysis of the interaction in DFT + DMFT calculations than was customary hitherto. Only if the oxygen degrees of freedom are included in the Wannier projection is this not necessary. In this case, however, the (different) d-p Coulomb interactions should be taken into account. For e_g orbitals there is no such difference between spherical and cubic interaction.

Depending on the screening length, screening enhances or reduces the difference between spherically symmetric and cubic interaction parameters. Screening can even enhance J whereas U and U' are always reduced. For Thomas–Fermi screening, $U = U' + 2J$ is still significantly violated for 5d BaOsO$_3$. Let us note that the simple Thomas–Fermi screening employed here is spherically symmetric, whereas the physical screening function obeys the cubic, not the spherical symmetry. This effect is an additional source of deviations from spherically symmetric interaction parameters.

For both e_g-only and t_{2g}-only low-energy effective models, we have a Kanamori interaction for cubic symmetry. This makes continuous-time quantum Monte Carlo simulations [37] very efficient because of an additional local symmetry; see Ref. [38].

APPENDIX A: COULOMB INTERACTION AND SLATER INTEGRALS

For the sake of completeness, let us briefly add the representation of the Coulomb interaction (1) by Slater integrals. Expressing

$$1/|\mathbf{r} - \mathbf{r}'| = \sum_{l,m} \frac{\min(r,r')^l}{\max(r,r')^{l+1}} \frac{4\pi}{2l+1} Y_{l,m}(\theta,\varphi) Y_{l,m}^*(\theta',\varphi')$$

in terms of spherical harmonics $Y_{l,m}$ and with $\psi_\alpha(\mathbf{r}) = R(r)Y_\alpha$ where $R(r)$ is independent of l (or α), the Coulomb interaction Eq. (1) becomes

$$U_{\alpha'\beta'\beta\alpha} = \frac{e^2}{4\pi\epsilon_0} \int dr\, d\Omega\, dr'\, d\Omega'\, R(r)Y_{\alpha'}(\theta,\varphi)R(r')Y_{\beta'}(\theta',\varphi')$$
$$\times \sum_{l,m} \left[\frac{\min(r,r')^l}{\max(r,r')^{l+1}} \frac{4\pi}{2l+1} Y_{l,m}(\theta,\varphi) Y_{l,m}(\theta',\varphi') \right]$$
$$\times R(r')Y_\beta(\theta',\varphi')R(r)Y_\alpha(\theta,\varphi)r'^2 r^2. \tag{A1}$$

This integral can be decomposed into a radial part ($dr\,dr'$) and an angular part ($d\Omega\,d\Omega'$), and the latter can be expressed in terms of Clebsch–Gordan coefficients. Thus, only the radial integrals (also known as Slater parameters) F_l of Eq. (2) need to be calculated.

TABLE V. Hopping amplitudes t between the three t_{2g} Wannier functions at various distances and their on-site energies E relative to the Fermi level. Values are in eV.

	$t_\pi^{(1)}$	$t_\delta^{(1)}$	$t_\sigma^{(2)}$	$t_\perp^{(2)}$	$t_\parallel^{(2)}$	E
SrVO$_3$	-0.263	-0.027	-0.084	0.009	0.006	0.580
BaOsO$_3$	-0.394	-0.043	-0.112	-0.012	0.013	-0.453

TABLE VI. Selected hopping amplitudes t between twelve-band Wannier functions and their on-site energies E relative to the Fermi level. Where the sign of the hopping alternates due to the signs of the p-type orbitals, we give the modulus. Values are in eV.

	$t_{dd\pi}^{(1)}$	$t_{dd\delta}^{(1)}$	$|t_{dp_\pi}|$	$|t_{p_\pi p_\pi}|$	$|t_{p_\pi p'_\pi}|$	$|t_{p_\pi p_\sigma}|$	$t_{p_\sigma p_\sigma}$	$t_{p_\pi p_\pi}^{(1)}$	$t_{p_\sigma p_\sigma}^{(1)}$	E_d	E_{p_π}	E_{p_σ}
SrVO$_3$	-0.128	-0.005	1.099	0.064	0.369	0.258	-0.044	-0.078	0.671	-0.407	-3.780	-5.520
BaOsO$_3$	-0.187	-0.002	1.240	0.007	0.204	0.195	-0.024	-0.107	0.903	-2.063	-3.896	-6.887

APPENDIX B: HOPPING MATRICES

In this appendix, we report the numerical values of selected hopping amplitudes in our Wannier projections [39]. The values for SrVO$_3$ may be compared with Refs. [24,26]. Note that this is not an enumeration of the largest hopping amplitudes; rather, the selection is meant to be illustrative.

For the three-band Wannier functions (values in Table V), no hopping is possible within the unit cell. Two nearest-neighbor hoppings are allowed, a π-type hopping $t_\pi^{(1)}$ when the displacement is in the same plane as the orbital lobes [e.g., xy orbitals with displacement (1 0 0)], and a smaller $t_\delta^{(1)}$ of δ type where the displacement is perpendicular [e.g., xy and (0 0 1)]. Interorbital nearest-neighbor hopping is forbidden by cubic symmetry. There are three second-nearest-neighbor hopping parameters: $t_\sigma^{(2)}$ when both orbitals and the displacement share a plane [e.g., xy and (1 1 0)]; $t_\parallel^{(2)}$ when the orbitals' planes are parallel [e.g., $xz \leftrightarrow xz$ and (1 1 0)]; and $t_\perp^{(2)}$ when the planes are perpendicular [e.g., $xz \leftrightarrow yz$ and (1 1 $\bar{0}$)].

For the twelve-band case (Table VI), we report the nearest-neighbor $d \leftrightarrow d$ hopping parameters $t_{dd}^{(1)}$ analogous to those of the three-band case, but not those to further neighbors. In any case, O-mediated hopping, which was subsumed in the hoppings of the three-band orbitals, now has to be taken into account explicitly.

Within the octahedron, the following hopping processes are possible: t_{dp_π} when the p_π orbital resides in the plane defined by the d (e.g., $d_{xy} \leftrightarrow p_y^{+x}$); $t_{p_\pi p_\pi}$ between nearest-O neighbors, i.e., along an edge of the octahedron (e.g., $p_y^{+x} \leftrightarrow p_y^{+z}$); $t_{p_\pi p'_\pi}$ which is the same as the last, but between orbitals of different orientation (e.g., $p_y^{+x} \leftrightarrow p_x^{+y}$); $t_{p_\pi p_\sigma}$ along an edge (e.g., $p_y^{+x} \leftrightarrow p_y^{+y}$); $t_{p_\sigma p_\sigma}$ along an edge (e.g., $p_x^{+x} \leftrightarrow p_y^{+y}$); $t_{p_\pi p_\pi}^{(1)}$ across the octahedron (e.g., $p_y^{+x} \leftrightarrow p_y^{-x}$); and $t_{p_\sigma p_\sigma}^{(1)}$ across the octahedron (e.g., $p_x^{+x} \leftrightarrow p_x^{-x}$).

Comparing the sequences of values for the two materials, the same trends are observed (with the exceptions of $t_\perp^{(2)} \gtrless t_\parallel^{(2)}$ and $|t_{p_\pi p_\pi}| \gtrless |t_{p\sigma p\sigma}|$). However, the values for the d-only orbitals, and for dd and pd processes in the twelve-band orbitals, are in general larger for BaOsO$_3$ than for SrVO$_3$, the larger lattice constant of BaOsO$_3$ notwithstanding (4.03 Å versus 3.84 Å for SrVO$_3$). This is reflective of the greater p-d hybridization and spatial extent of the $5d$ states.

Contrariwise, the twelve-band pp hopping processes have larger amplitude in SrVO$_3$. Our interpretation is that, in this case, the larger spatial distance prevails; indeed, the difference in Wannier-function spread $\langle r^2 \rangle$ between SrVO$_3$ and BaOsO$_3$ is much more pronounced for the d than for the p orbitals. The exceptions to this rule, $t_{p_\pi p_\pi}^{(1)}$ and $t_{p_\sigma p_\sigma}^{(1)}$ (hopping across the octahedron), may be explained by the stronger p-d hybridization in BaOsO$_3$.

[1] J. G. Bednorz and K. A. Müller, Z. Phys. B: Condens. Matter **64**, 189 (1986); Y. Kamihara, T. Watanabe, M. Hirano, and H. Hosono, J. Am. Chem. Soc. **130**, 3296 (2008).

[2] P. Coleman and A. J. Schofield, Nature **433**, 226 (2005).

[3] V. I. Anisimov, J. Zaanen, and O. K. Andersen, Phys. Rev. B **44**, 943 (1991).

[4] V. I. Anisimov, A. I. Poteryaev, M. A. Korotin, A. O. Anokhin, and G. Kotliar, J. Phys.: Condens. Matter **9**, 7359 (1997); A. I. Lichtenstein and M. I. Katsnelson, Phys. Rev. B **57**, 6884 (1998); K. Held, I. A. Nekrasov, G. Keller, V. Eyert, N. Blümer, A. McMahan, R. Scalettar, T. Pruschke, V. I. Anisimov, and D. Vollhardt, Phys. Status Solidi B **243**, 2599 (2006); G. Kotliar, S. Y. Savrasov, K. Haule, V. S. Oudovenko, O. Parcollet, and C. A. Marianetti, Rev. Mod. Phys. **78**, 865 (2006); K. Held, Adv. Phys. **56**, 829 (2007).

[5] G. H. Wannier, Phys. Rev. **52**, 191 (1937).

[6] E. Müller-Hartmann, Z. Phys. B: Condens. Matter **74**, 507 (1989).

[7] N. Parragh, G. Sangiovanni, P. Hansmann, S. Hummel, K. Held, and A. Toschi, Phys. Rev. B **88**, 195116 (2013).

[8] J. C. Slater, *Quantum Theory of Atomic Structure* (McGraw-Hill, New York, 1960); J. S. Griffith, *The Theory of Transition-Metal Ions* (Cambridge University Press, Cambridge, 1971).

[9] J. Kanamori, Prog. Theor. Phys. **30**, 275 (1963).

[10] See, among others, [3]; P. Blaha, K. Schwarz, G. Madsen, D. Kvasnicka, J. Luitz, User's Guide, Wien2K_13.1 [www.wien2k.at/reg_user/textbooks]; Jan Kunes, Alexey V. Lukoyanov, Vladimir I. Anisimov, Richard T. Scalettar, and Warren E. Pickett, Nat. Mater. **7**, 198 (2008); E. Assmann, P. Blaha, R. Laskowski, K. Held, S. Okamoto, and Giorgio Sangiovanni, Phys. Rev. Lett. **110**, 078701 (2013); C. Franchini, R. Kovacik, M. Marsman, S. Sathyanarayana Murthy, J. He, C. Ederer, and G. Kresse, J. Phys.: Condens. Matter **24**, 235602 (2012); A. A. Tsirlin, O. Janson, and H. Rosner, Phys. Rev. B **84**, 144429 (2011); E. R. Ylvisaker, W. E. Pickett, and K. Koepernik, *ibid.* **79**, 035103 (2009).

[11] In DFT + DMFT usually Kanamori interaction parameters are used; see, among others, K. Haule, C.-H. Yee, and K. Kim, Phys. Rev. B **81**, 195107 (2010); I. Di Marco, P. Thunström, M. I. Katsnelson, J. Sadowski, K. Karlsson, S. Lebègue, J. Kanski, and O. Eriksson, Nat. Commun. **4**, 2645 (2013); P. Hansmann, A. Toschi, G. Sangiovanni, T. Saha-Dasgupta, S. Lupi, M. Marsi, and K. Held, Phys. Status Solidi B **250**, 1251 (2013); S. Backes, D. Guterding, H. O. Jeschke, and R. Valenti, New J. Phys. **16**, 083025 (2014); Z. Zhong, M. Wallerberger, J. M. Tomczak, C. Taranto,

N. Parragh, A. Toschi, G. Sangiovanni, and K. Held, arXiv:1312.5989; G. Giovannetti, M. Aichhorn, and M. Capone, arXiv:1402.0901; H. T. Dang, X. Ai, A. J. Millis, and C. A. Marianetti, Phys. Rev. B **90**, 125114 (2014).

[12] L. de'Medici, J. Mravlje, and A. Georges, Phys. Rev. Lett. **107**, 256401 (2011).

[13] For DFT + DMFT calculations with Slater integrals see, e.g., P. Thunström, I. Di Marco, O. Eriksson, Phys. Rev. Lett. **109**, 186401 (2012); R. Arita, J. Kunes, A. V. Kozhevnikov, A. G. Eguiluz, and M. Imada, *ibid.* **108**, 086403 (2012).

[14] C. J. Ballhausen, *Introduction to Ligand Field Theory* (McGraw-Hill, New York, 1962).

[15] M. W. Haverkort, M. Zwierzycki, and O. K. Andersen, Phys. Rev. B **85**, 165113 (2012); N. Rezaei, P. Hansmann, M. S. Bahramy, and R. Arita, *ibid.* **89**, 125125 (2014).

[16] Note that, in the constrained random phase approximation [40], one can in principle and sometimes does calculate the full Coulomb interaction matrix. However, usually the subsequent DMFT calculation only employs Slater or Kanamori parameters; if not, a Kanamori parametrization is assumed from the very beginning [41].

[17] See, e.g., G. F. Koster, J. O. Dimmock, R. G. Wheeler, and H. Statz, *Properties of the Thirty-Two Point Groups* (MIT Press, Cambridge, 1963).

[18] M. Imada, A. Fujimori, and Y. Tokura, Rev. Mod. Phys. **70**, 1039 (1998).

[19] A. Georges, L. de'Medici, and J. Mravlje, Annu. Rev. Condens. Matter Phys. **4**, 137 (2013); S. Sugano, Y. Tanabe, and H. Kamimura, *Multiplets of Transition-Metal Ions in Crystals* (Academic Press, New York, 1970).

[20] Note that, without the e_g orbitals, the Hamiltonian itself is actually not spherically symmetric. Rotation of, e.g., the d_{xy} orbital around the z axis maps it onto a linear combination involving (missing) e_g orbitals; rotating it around the x or y axis maps it onto a linear combination of the (included) t_{2g}. The Hamiltonian is invariant under the latter rotations if $U = U' + 2J$.

[21] P. Blaha, K. Schwarz, G. K. H. Madsen, D. Kvasnicka, and J. Luitz, *WIEN2k, An Augmented Plane Wave + Local Orbitals Program for Calculating Crystal Properties* (Techn. Universität Wien, Vienna, Austria, 2001).

[22] J. P. Perdew, K. Burke, and M. Ernzerhof, Phys. Rev. Lett. **77**, 3865 (1996).

[23] A. A. Mostofi, J. R. Yates, Y.-S. Lee, I. Souza, D. Vanderbilt, and N. Marzari, Comput. Phys. Commun. **178**, 685 (2008); N. Marzari, A. A. Mostofi, J. R. Yates, I. Souza, and D. Vanderbilt, Rev. Mod. Phys. **84**, 1419 (2012).

[24] J. Kuneš, R. Arita, P. Wissgott, A. Toschi, H. Ikeda, and K. Held, Comput. Phys. Commun. **181**, 1888 (2010).

[25] A. Sekiyama, H. Fujiwara, S. Imada, S. Suga, H. Eisaki, S. I. Uchida, K. Takegahara, H. Harima, Y. Saitoh, I. A. Nekrasov, G. Keller, D. E. Kondakov, A. V. Kozhevnikov, Th. Pruschke, K. Held, D. Vollhardt, and V. I. Anisimov, Phys. Rev. Lett. **93**, 156402 (2004); E. Pavarini, S. Biermann, A. Poteryaev, A. I.

Lichtenstein, A. Georges, and O. K. Andersen, *ibid.* **92**, 176403 (2004); A. Liebsch, *ibid.* **90**, 096401 (2003); I. A. Nekrasov, G. Keller, D. E. Kondakov, A. V. Kozhevnikov, T. Pruschke, K. Held, D. Vollhardt, and V. I. Anisimov, Phys. Rev. B **72**, 155106 (2005).

[26] E. Pavarini, A. Yamasaki, J. Nuss, and O. K. Andersen, New J. Phys. **7**, 188 (2005).

[27] A. Scaramucci, J. Ammann, N. A. Spaldin, and C. Ederer, arXiv:1405.3804.

[28] Y. Shi, Y. Guo, Y. Shirako, W. Yi, X. Wang, A. A. Belik, Y. Matsushita, H. L. Feng, and Y. Tsujimoto, M. Arai *et al.*, J. Am. Chem. Soc. **135**, 16507 (2013).

[29] P. Hansmann, N. Parragh, A. Toschi, G. Sangiovanni, and K. Held, New J. Phys. **16**, 033009 (2014).

[30] Z. Zhong, A. Toth, and K. Held, Phys. Rev. B **87**, 161102(R) (2013).

[31] Note that t in Eq. (5) is $|t| \sim 2|t_{dp_\pi}|$ since the former denotes the hopping between d and O orbitals, and the latter between d and p.

[32] We checked for convergence and errors with respect to the number of Wannierization k points, the size of the real-space cell, the number of real-space support points, and shifts of these support points. The accuracy of integrals is $\lesssim 0.2\%$.

[33] J. Mravlje, M. Aichhorn, T. Miyake, K. Haule, G. Kotliar, and A. Georges, Phys. Rev. Lett. **106**, 096401 (2011).

[34] L. Vaugier, H. Jiang, and Silke Biermann, Phys. Rev. B **86**, 165105 (2012).

[35] Y. C. Lan, X. L. Chen, and A. He, J. Alloys Compd. **354**, 95 (2003).

[36] K. Haule and G. Kotliar, New J. Phys. **11**, 025021 (2011).

[37] A. N. Rubtsov and A. I. Lichtenstein, JETP Lett. **80**, 61 (2004); P. Werner, A. Comanac, L. de'Medici, M. Troyer, and A. J. Millis, Phys. Rev. Lett. **97**, 076405 (2006); E. Gull, P. Werner, O. Parcollet, and M. Troyer, Europhys. Lett. **82**, 57003 (2008); E. Gull, A. J. Mills, A. I. Lichtenstein, A. N. Rubtsov, M. Troyer, and P. Werner, Rev. Mod. Phys. **83**, 349 (2011).

[38] N. Parragh, A. Toschi, K. Held, and G. Sangiovanni, Phys. Rev. B **86**, 155158 (2012).

[39] The signs of the hopping amplitudes reported here are as they would appear in a Hamiltonian matrix, i.e., without the extra sign of "$-t$."

[40] F. Aryasetiawan, M. Imada, A. Georges, G. Kotliar, S. Biermann, and A. I. Lichtenstein, Phys. Rev. B **70**, 195104 (2004); T. Miyake, F. Aryasetiawan, and M. Imada, *ibid.* **80**, 155134 (2009); M. Hirayama, T. Miyake, and M. Imada, *ibid.* **87**, 195144 (2013); M. Imada and T. Miyake, J. Phys. Soc. Jpn. **79**, 112001 (2010).

[41] J. M. Tomczak, M. Casula, T. Miyake, F. Aryasetiawan, and S. Biermann, Europhys. Lett. **100**, 67001 (2012); C. Taranto, M. Kaltak, N. Parragh, G. Sangiovanni, G. Kresse, A. Toschi, and K. Held, Phys. Rev. B **88**, 165119 (2013); M. Hirayama, T. Miyake, and M. Imada, *ibid.* **87**, 195144 (2013).